Supporting Information

Cho et al. 10.1073/pnas.1002716107

Cho et al. 10.1073/pnas.1002716107

SI Text

SI Methods. ***Phosphodiesterase inhibition studies.*** Using recombinant human phosphodiesterase enzymes expressed and purified in a baculoviral system as previously described (1), AV411 (ibudilast, 3-isobutyryl-2-isopropylpyrazolo-[1,5-a]pyridine) and AV1013 were assayed for inhibition of conversion of ^{3}H-cAMP to ^{3}H-AMP or ^{3}H-cGMP to ^{3}H-GMP using a modification of the two-step method of Thompson and Appleman (2) adapted for 96 well plate format. The assay contained one unit of enzyme (amount of enzyme that converts 1 pmole cAMP to AMP, or cGMP to GMP per min at pH 7.5 at 30 °C) and the compounds were dissolved in 5% DMSO to a concentration of 10 μM. The data are expressed as percent inhibition of each phosphodiesterase (PDE) isoform at 10 μM, and is a mean of duplicate datapoints.

Enzymatic and chemotactic inhibition assays. *p*-Hydroxyphenylpyruvate (HPP) tautomerization experiments were performed at 306 nm in triplicate. Inhibition constants were determined by nonlinear regression against noncompetitive and competitive equations using Prism4 (GRAPHPAD).

For cellular assays, various concentrations of AV411 or AV1013 were incubated with 8 nM macrophage migration inhibitory factor (MIF) in peripheral blood mononuclear cell (PBMC) migration experiments (3). Control experiments were also carried out using recombinant MIP-1α (8 nM; Pierce) as well as IL-8 (8 nM; eBioscience) and a dilution series of AV411 and AV1013 (both R and S enantiomers). Blocking antibodies to human CXCR2 (R&D Systems), CXCR4 (R&D Systems), and CD74 (BD Pharmingen) were used alone or in combination at a concentration of 10 μg/mL. In these antibody assays, PBMCs were incubated with antibodies for 30 min at 37 °C in RPMI medium 1640 prior to their use. Results are expressed as the mean number of cells counted per high-power field for each of more than two fields ± SEM.

Fluorescence spectroscopy. Assays were performed in 0.424 M borate to make the aqueous condition consistent with that for enzyme kinetics. Base lines for each inhibitor at different concentrations were established with inhibitor alone in the assay buffer. Fluorescence quenching experiments were done by 814 Photomultiplier Detection System (Photon Technology International, Inc.) using the acquisition program LabWork provided by the manufacturer. Three repeats of assay for each inhibitor were linearly regressed by Prism.

NMR spectroscopy. For the AV411 heteronuclear single quantum coherence (HSQC) experiment, reference (no inhibitor) and inhibitor-containing samples were prepared by mixing 700 μL of ^{15}N-labeled rhMIF (400 μM) and 78 μL of D_2O, splitting it in half into two NMR tubes, and adding 4.2 μL of 100% DMSO and 50 mM AV411 (in 100% DMSO), respectively. For the AV1013 transverse relaxation optimized spectroscopy (TROSY) experiments, 200 μM of ^{15}N-labeled rhMIF with 10% D_2O was mixed with either 88 μL of 50 mM of AV1013 or the same volume of DMSO as a reference. All of the experiments were carried out at 25 ºC in a Varian INOVA 600 MHz spectrometer with a 5-mm triple resonance probe equipped with triple-axis (*xyz*) pulsed magnetic field gradients. Spectra were processed and analyzed using the software programs nmrPipe (4) and Sparky (http://www.cgl.ucsf.edu/home/sparky/).

X-ray crystallography. MIF was cocrystallized with (*R*)-AV1013 using the hanging drop vapor diffusion method. A solution containing 1.1 mM MIF and 5 mM (*R*)-AV1013 in 10% DMSO, 18 mM Tris (pH 7.5), 18 mM NaCl was mixed 1:1 with reservoir solution containing 2 M $(NH_4)_2SO_4$, 0.5 M NaCl, 0.1 M Tris (pH 7.5), 3% isopropanol, and incubated at 37 °C. For the ternary complex of MIF with both HPP and (*R*)-AV1013, a solution of 1.0 mM MIF, 5 mM (*R*)-AV1013, 10 mM HPP in 10% DMSO, 0.1 M acetate (pH 6.0), 14 mM Tris, 14 mM NaCl was mixed 1:1 with the same reservoir solution. Each crystal was soaked in cryoprotectant solution containing 3 M NaCl, 2 M $(NH_4)_2SO_4$, 50 mM Tris (pH 7.5). For the binary complex crystal, data were collected on a Rigaku micromax generator with an R-Axis IV image-plate detector. Data from a crystal of MIF/(*R*)-AV1013/HPP were collected at beamline X29 of the National Synchrotron Light Source at Brookhaven National Laboratory. Diffraction data were processed using HKL2000. The structures were determined by molecular replacement using unliganded MIF (PDB 3DJH) (5). In each structure, (*R*)-AV1013 is bound in only one of three allosteric sites due to crystal packing. HPP is found in all three active sites of the ternary complex. Refinement was performed using the programs CNS (6), ShelxL (7), and REFMAC (8). The dihedral and bond angle parameters in the dictionary files were relaxed for one of the HPP forms in the inhibited site to fit the 1.25 Å electron density. Manual adjustments to the model were made using O (9) and COOT (10).

Synthesis and resolution of AV1013 (Scheme S1).

Step 1: Benzyl 1-(methoxy(methyl)amino)-1-oxopropan-2-yl carbamate. (R, S)-2-Benzyloxycarbonylamino-propionic acid (12.15 g, 54.4 mmol), diisopropylethylamine (28.4 mL, 163.3 mmol), (benzotriazol-1-yloxy)tris(dimethylamino)phosphonium hexafluorophosphate (BOP Reagent) (28.89 g, 65.3 mmol), and tetrahydrofuran (THF) (300 mL) were combined and stirred at 0° C. N,O-dimethylhydroxylamine hydrochloride (6.37 g, 65.3 mmol) was added to the mixture, and the reaction was stirred for 18 h. The reaction was quenched with saturated ammonium chloride solution and extracted with ethyl acetate. The organic layer was dried over sodium sulfate, filtered, and concentrated in vacuo. The crude material was purified by silica gel flash chromatography (0–60% ethyl acetate in hexanes) to give 13.48 g (93%) of benzyl 1-(methoxy(methyl)amino)-1-oxopropan-2-yl carbamate.

Step 2: Benzyl 6-methyl-3-oxohept-4-yn-2-yl carbamate.
3,3-Dimethyl-but-1-yne (68.5 mL, 1.00 mole) was dissolved in THF (1 L), and the solution was cooled to −78 °C. n-butyllithium (2.5 M in hexanes, 300 mL, 750 mmol) was slowly added to a stirred solution, at a rate that maintained a temperature below −65 °C. The reaction mixture was stirred for 30 min, and a solution of benzyl 1-(methoxy(methyl)amino)-1-oxopropan-2-yl carbamate (41.4 g, 156 mmol) in THF (1 L) was slowly added to the stirring reaction mixture, at a rate that maintained a temperature below −65 °C. The combined reaction mixture was stirred at −78 °C for 1 h. The reaction was quenched by pouring into saturated ammonium chloride solution and extracted with ethyl acetate. The organic layer was dried over sodium sulfate and concentrated in vacuo. The crude material (43.32 g, 102%) was used in the next step without further purification, because of limited stability.

Step 3: Benzyl 1-(2-isopropylpyrazolo[1,5-a]pyridin-3-yl)-1-oxopropan-2-yl carbamate.
Benzyl 6-methyl-3-oxohept-4-yn-2-yl carbamate (43.32 g, 158.5 mmol), 1-aminopyridinium iodide (36.00 g, 162.1 mmol), and dry acetonitrile (1 L) were combined and stirred at room temperature. 1,8-Diazabicyclo[5.4.0]undec-7-ene (70.0 mL, 468.1 mmol) was added slowly over a course of 30 min. The purple solution was allowed to stir at room temperature for 18 h. The reaction mixture was concentrated in vacuo, dissolved in dichloromethane, filtered through Celite, and concentrated again. The crude material was purified by silica gel flash chromatography (0–60% ethyl acetate in hexanes) and recrystallized with ethyl acetate and hexanes to give 13.68 g (24%) of benzyl 1-(2-isopropylpyrazolo[1,5-a]pyridin-3-yl)-1-oxopropan-2-yl carbamate as a white crystalline powder.

Step 4: Resolution of [2-(2-Isopropyl-pyrazolo[1,5-a]pyridin-3-yl)-1-methyl-2-oxo-ethyl]-carbamic acid benzyl ester.
The racemic mixture was separated into individual enantiomers using a ChiralPak AY chiral column (Chiral Technologies) using 100% acetonitirile as the eluent.

Step 5: Racemic, (R)- and (S)-2-amino-1-(2-isopropylpyrazolo[1,5-a]pyridin-3-yl)propan-1-one hydrochloride.
A racemic mixture, or individual enantiomers, of [2-(2-isopropyl-pyrazolo[1,5-a]pyridin-3-yl)-1-methyl-2-oxo-ethyl]-carbamic acid benzyl ester (1.00 g, 2.74 mmol) and Pd on carbon (5%, 58 mg, 0.03 mmol) were mixed in absolute ethanol (120 mL). The reaction flask was purged with hydrogen, and HCl in ethanol (1.25 M, 6.0 mL; Aldrich/Fluka) was added. The reaction was run under 1 atm of hydrogen and monitored by HPLC-MS (~5 h reaction time). Care was taken to avoid overreduction of the pyrazolo[1,5-a]pyridine ring, and the reaction was stopped at approximately 90% completion. The reaction mixture was filtered through Celite, and the solution was concentrated in vacuo. The crude material was dissolved in water and washed twice with ethyl acetate. The water layer was concentrated in vacuo and lyophilized to furnish 550 mg (75% yield) of racemic or (R)- or (S)-2-amino-1-(2-isopropylpyrazolo[1,5-a]pyridin-3-yl)propan-1-one hydrochloride. Chemical purity >98% by RP-HPLC with UV (254 nm), evaporative light scattering detector and MS detection $M + H$ 232. Chiral purity was determined by HPLC using a chiral column, Chiral-AGP 100×4.0 mm, 5 μm (from ChromTech) using 5% acetonitrile and ammonium acetate buffer (25 mM) as eluent. NMR (^{1}H, D_6-DMSO, 300 MHz): 8.91 (d, 1H); 8.43 (broad s, 3H); 8.06 (d, 1H); 7.71 (t, 1H); 7.21 (t, 1H); 4.8 (m, 1H); 3.69 (m, 1H); 1.44 (d, 3H); 1.36 (d, 3H); 1.29 (d, 3H).

1. Gibson LC, et al. (2006) The inhibitory profile of ibudilast against the human phosphodiesterase enzyme family. *Eur J Pharmacol* 538:39–42.
2. Thompson WJ, Appleman MM (1971) Multiple cyclic nucleotide phosphodiesterase activities from rat brain. *Biochemistry* 10:311–316.
3. Cho Y, et al. (2007) Structural and functional characterization of a secreted hookworm Macrophage Migration Inhibitory Factor (MIF) that interacts with the human MIF receptor CD74. *J Biol Chem* 282:23447–23456.
4. Delaglio F, et al. (1995) NMRPipe: A multidimensional spectral processing system based on UNIX pipes. *J Biomol NMR* 6:277–293.
5. Crichlow GV, Lubetsky JB, Leng L, Bucala R, Lolis EJ (2009) Structural and kinetic analyses of macrophage migration inhibitory factor active site interactions. *Biochemistry* 48:132–139.
6. Brunger AT, et al. (1998) Crystallography & NMR system: A new software suite for macromolecular structure determination. *Acta Crystallogr D* 54:905–921.
7. Sheldrick G (2008) A short history of SHELX. *Acta Crystallogr A* 64:112–122.
8. Murshudov GN, Vagin AA, Dodson EJ (1997) Refinement of macromolecular structures by the maximum-likelihood method. *Acta Crystallogr D* 53:240–255.
9. Jones TA, Zou JY, Cowan SW, Kjeldgaard M (1991) Improved methods for building protein models in electron density maps and the location of errors in these models. *Acta Crystallogr. A* 47:110–119.
10. Emsley P, Cowtan K (2004) Coot: Model-building tools for molecular graphics. *Acta Crystallogr D* 60:2126–2132.

Fig. S1. PBMC cell migration inhibition. (*A*) PBMC migration dose-response for (*S*)-AV1013. Positive control is with rhMIF but no drug added "0." Inhibitors (INH) is (*S*)-AV1013. P values represent significant difference relative to positive control. For all panels, negative control (NEG) is without rhMIF. (*B*) Comparison of MIF and MIP-1α chemotaxis in the presence of AV411 and AV1013. P values reflect comparison between the effect of inhibitors on MIF and MIP1α. NEG 411 and NEG 1013 are with drug alone. (*C*) IL-8 mediated chemotactic assay. Migration of PBMC was mediated by 8 nM IL-8 either in the absence or presence of 80 nM AV411. (*D*) Effect of AV411 on PDE inhibition: 411 (top), AV411 in the upper chamber; MIF (bot), MIF in the bottom chamber. (*E*) Inhibition of MIF-induced chemotaxis of PBMCs in the presence of three monoclonal antibodies (10 μg/mL each) directed against MIF receptors (CD74, CXCR2, and CXCR4). P values represent comparison to the MIF-mediated migration in the absence of the antibodies.

Fig. S2. AV411 and AV1013 interactions with rhMIF in solution. Chemical shift changes were described as large when less than half of the chemical shift overlapped with that of apo-rhMIF, and moderate when more than half of the chemical shift overlapped (Table S2). Residues revealing large chemical shift change are labeled in bold, whereas those revealing moderate chemical shift change are labeled with plain print. (*A*) Full-range HSQC spectra of MIF in the presence (red) or absence (blue) of AV411. (*B*) Full-range TROSY spectra of MIF in the presence (increasing concentration by strength of color) or absence (green) of AV1013. (*C*) A zoomed view of *B* showing large chemical shifts. (*D*) The surface of a rhMIF trimer is shown with the degree of chemical shift change, colored in red after scaled to those of AV411, upon binding of AV1013. On the right is shown the rotated and clipped surface of trimer.

Fig. S3. Extension of Phe113 into the inhibited active site. The predominant rotamer of the Phe113 side chain in the inhibited active site approaches the keto/enol oxygen of the Pro1 proximal HPP. Subunit A was overlaid onto subunit C by least-squares superposition of α-carbons of residues 2–15, 17–32, and 38–112 of chain A onto equivalent α-carbons in chain C. Carbon atoms of HPP are colored in cyan (enol form) and in gray (Pro1 proximal form). Phe113 from the inhibited active site is in green carbon atoms, and in yellow is Phe113 from an uninhibited active site.

Table S1. Percent inhibition of AV411 and AV1013 at 10 μM against pure recombinant human PDE isozymes

PDE isozyme	AV411	AV1013
PDE3 (cAMP)	25	5
PDE4 (cAMP)	57	1
PDE10 (cAMP)	66	15
PDE10 (cGMP)	81	27
PDE11 (cAMP)	40	14
PDE11 (cGMP)	30	11

Table S2. Inhibition of MIF-induced migration of human PBMCs by monoclonal antibodies directed against MIF receptors

Assay	Avg no. of migrated cells	% enhancement of migration relative to MIF alone [(assay-Neg)/(MIF-Neg) × 100]	% inhibition	P value (relative to MIF alone in the same experiment)
Experiment no. 1 (Fig. 2*C*)				
Negative control	53.17	0.0		<0.01
MIF	108.3	100.0		
α-CD74	110.0	103.1	−3.1	>0.05
α-CXCR2	70.50	31.4	68.6	<0.01
α-CXCR4	83.50	55.0	45.0	>0.05
α-CD74/α-CXCR2	74.17	38.1	61.9	<0.05
α-CD74/α-CXCR4	82.17	52.6	47.4	>0.05
α-CXCR2/α-CXCR4	65.17	21.8	78.2	<0.01
Experiment no. 2 (Fig. S1*D*)				
Negative control	51.83	0.0		<0.01
MIF	142.2	100.0		
MIF + 3Abs	72.00	22.3	77.7	<0.01

Table S3. Residues with large and moderate NMR chemical shift changes in the presence of each inhibitor

	Large shifts	Moderate shifts
AV411	F3, Q35, Y36*, A38, G50, H62, S63, I64, G65, K66, I67, N72, G107, N109, T112, F113	M2, N6, Q28, T30, G31, K32, V39, H40, V41, D44, M47, F49, G51, S60, S74, L87, I89, R93, Y98, D100, N102, N105, S111
AV1013	S20, Q35, Y36, H62, I64, N109, T112	Q28, T30, I37, F49, G50, G51, E54, S63, K66, I67, R73, C80, R93, V94, Y98, D100, N105, G107, W108, F113

*Common residues between the two inhibitors are underlined.

Table S4. Crystallographic statistics of the MIF-AV1013 and MIF-AV1013-HPP structures

	MIF/(*R*)-AV1013	MIF/(*R*)-AV1013/HPP
Data collection		
Space group	$P2_12_12_1$	$P2_12_12_1$
Cell dimensions		
a, *b*, *c*, Å	66.96, 68.04, 87.28	67.24, 67.91, 87.33
α, β, γ, °	90, 90, 90	90, 90, 90
Resolution, Å	1.70 (1.73-1.70) *	1.25 (1.27-1.25)
R_{sys} or R_{merge}	0.073 (0.514)	0.064 (0.475)
I/σ	21.7 (2.02)	26.7 (2.61)
Completeness, %	99.5 (96.0)	99.9 (100.0)
Redundancy	4.3 (3.7)	4.8 (4.7)
Refinement		
Resolution, Å	1.70	1.25
No. reflections	42,687	110,630
R_{work}/R_{free}	0.194/0.206	0.162/0.185
No. atoms		
Protein	2,604	2,647
Ligand/ion	27	103
Water	393	486
B factors		
Protein	20.62	14.24
Ligand/ion	51.92	29.33
Water	31.64	28.79
rms deviations		
Bond lengths, Å	0.005	0.006
Bond angles, °	1.3	1.2

Data were collected on one crystal for each structure.
*Values in parentheses are for highest-resolution shell.

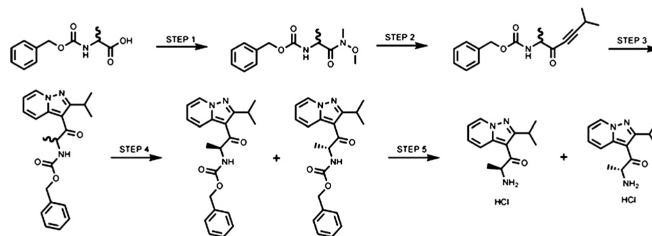

Scheme S1. Synthesis and resolution of AV1013

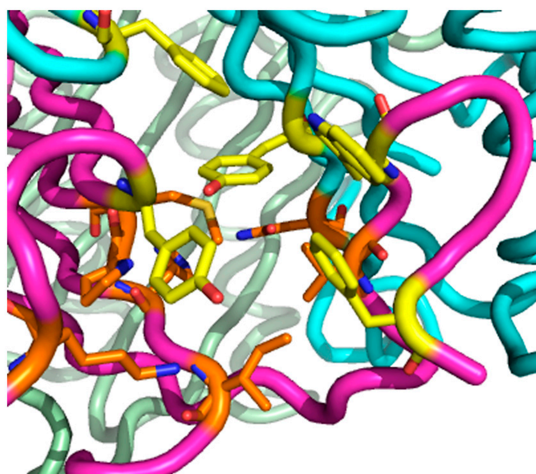

Movie S1. Conformational change of MIF, which leads to the formation of an induced allosteric binding site, upon binding of HPP and AV1013R was generated by morphing from an unbound MIF (PDB ID code 1MIF) to a ternary complex state MIF/HPP/AV1013R (PDB ID code 3IJJ).

Movie S1 (MOV)